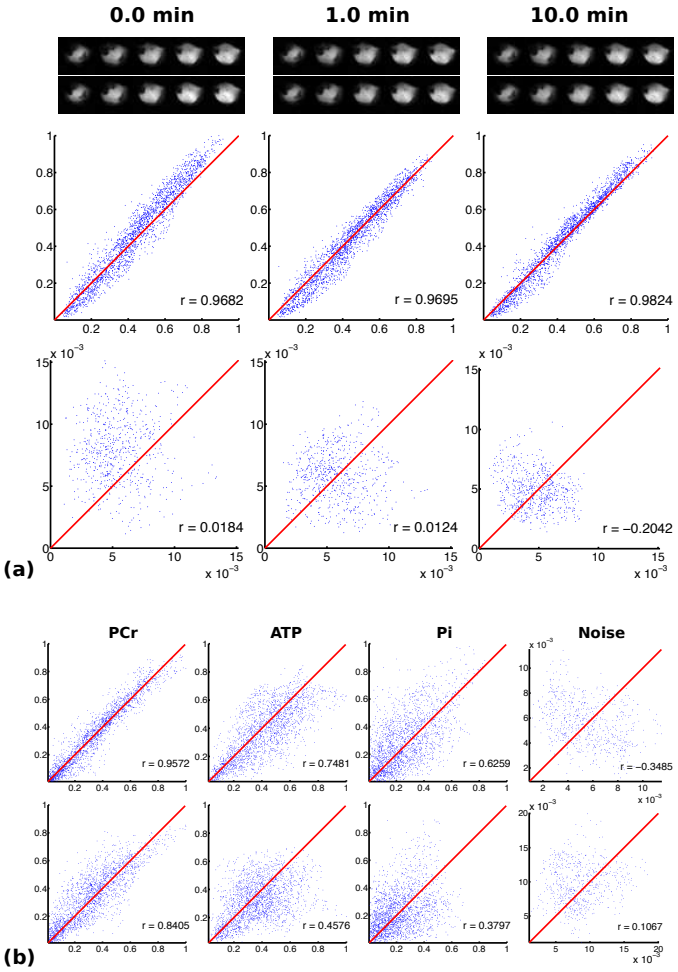

Fig. S2. Reproducibility of *in vivo* measurements of metabolite concentration dynamics from two rounds of control experiments performed on the same animal. The layout of (a) is the same as that of Fig. 4, and the layout of (b) is the same as that of Fig. 5.

VII. Supplemental Material

Fig. S1. Video of the estimated PCr and Pi distributions over time from two rounds (left and right columns) of stimulation-recovery experiments performed on the same animal. The average spectrum over time from the leg is shown in black (third row) and two selected localized spectra over time are shown below (rows 4 and 5, respectively). The locations of the localized spectra are indicated by color-coded markers in the PCr distributions.

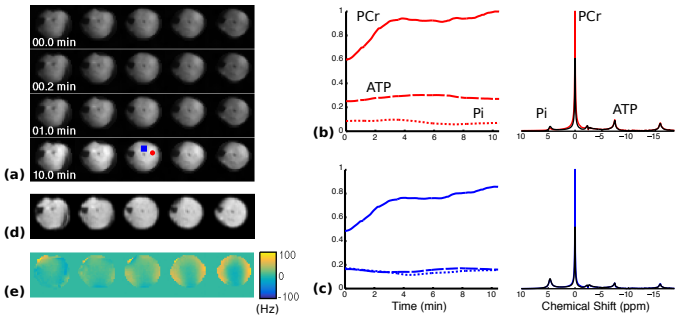

Fig. S3. Reconstruction of dynamic MRSI data from rat hindlimb during stimulation-recovery generated using the same temporal subspace estimation method used to reconstruct the control experiment data in Fig. 6. The figure layout is the same as that of Fig. 2.

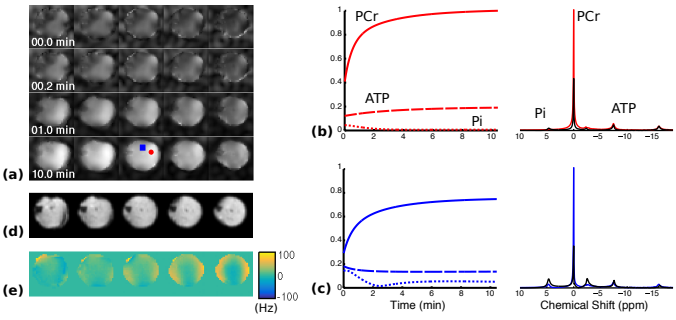

Fig. S4. Reconstruction of dynamic MRSI data from rat hindlimb during stimulation-recovery performed with $r_m(\boldsymbol{x})$ set to one. The layout of this figure is the same as that of Fig. 2.

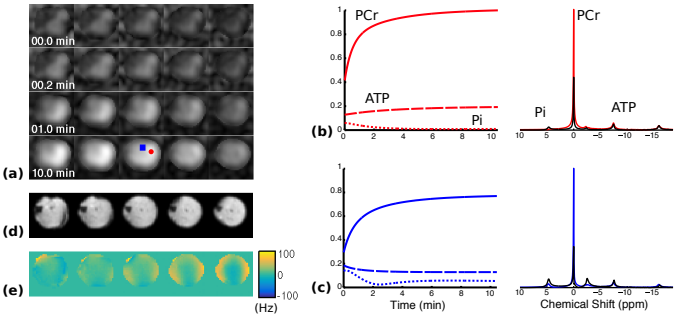

Fig. S5. Reconstruction of dynamic MRSI data from rat hindlimb during stimulation-recovery performed with $r_m(\boldsymbol{x})$ and the weights in the regularization set to one. The layout of this figure is the same as that of Fig. 2.

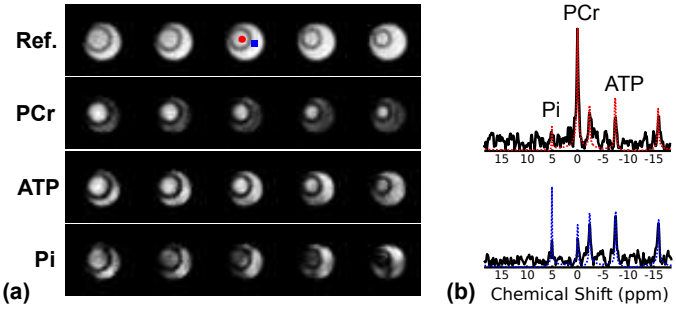

Fig. S6. Phantom validation of metabolic mapping. (a) Reference ^{1}H image and PCr, ATP, and Pi concentration maps from the average of 64 frames (82 s acquisition). (b) Reconstructed spectra (dotted-colored lines) as well as corresponding spectra from the reconstruction of the CSI training data (black lines) from two voxels indicated by the color-coded markers in the top row of (a).